Inorganic Chemistry Research

Article

Templated sol-gel Sr_2TiO_4 nanoparticle preparation as photocatalyst: Morphological-depended efficiency in organic dyes degradation

Elnaz Rashtizadeh[a,*], Zeinab Asgharpour[b]

[a]*Department of Chemistry Education, Farhangian University, P.O. Box 14665-889, Tehran, Iran*
[b]*Department of Chemistry, University of Alzahra, Vanak, Tehran, Iran*

Received: January 6, 2025; Accepted: January 18, 2025
Cite This: *Inorg. Chem. Res.* **2024**, *8*, 91-99. DOI: 10.22036/j10.22036.2025.498333.1179

Abstract: Semiconductor photocatalysts can effectively break down organic dye pollution. The degradation of Congo red and methylene blue by photocatalysis using a perovskite Sr_2TiO_4 nano-photocatalyst was investigated in this work. The nanostructure preparation method and template on photocatalytic efficiency were investigated. Results showed a correspondence of efficiency and procedure-based morphology. The catalyst was then examined using XRD, BET, FT-IR, SEM, and TGA/DTA. Under UV light irradiation, the Sr_2TiO_4 nanoparticle's photocatalytic activity was assessed. At room temperature, 5 ppm of Sr_2TiO_4 nano-photocatalyst dose, 50.0 mg/L initial dye concentration, and 60 minutes of irradiation time, degradation efficiencies of 94.0% for Congo red and 97.0% for methylene blue were attained. This photocatalyzed reaction exhibits a first-order behavior. For Congo red and methylene blue, the degradation rate constants were investigated. The investigation demonstrated that Sr_2TiO_4 nano-photocatalyst offers a high potential for methylene blue and Congo red photocatalytic degradation.

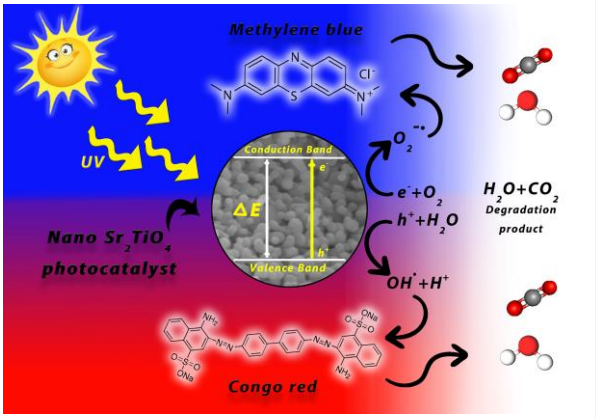

Keywords: Nano Sr_2TiO_4, Photocatalyst, Congo red, Methylene blue, Template

1. INTRODUCTION

One of the destructive problems that human society has imposed on the environment and trying to solve is surface water pollution by industrial activities.[1] One of the main culprits of water pollution are dyeing industry which about 1-20% of their organic dyes after use enter the environment. Textile dyeing, paper making, fabrics, furniture, clothing, plastics and pharmaceutical industries, paints, cosmetics including varnish and food processing industries are among the sources of discharge of dye effluents.[2-4] The discharge of dyes in surface waters causes oxygen depletion and reduces sunlight reaching underwater, reducing photosynthesis in aquatic plants.[5] Some organic dyes are toxic, carcinogenic, and harmful to the environment.[6] Most organic dyes consist of two main parts: chromophores responsible for light-absorbing properties and auxochromes allowing the dyes to bind onto substrates such as textile fibers.[7] Some dyes are soluble in water and are classified as cationic, anionic, or non-ionic.[8] Methylene blue (MB), a cationic thiazine dye, is one of the most widely used dyes in wood, cotton, silk, and pharmaceutical industries.[9-11] On the other hand, MB leads to health diseases such as nausea, necrosis, vomiting, diarrhea, eye irritation, breathing problems, and profuse sweating. As a result, it is very important to remove MB dye from the wastewater.[10,11] Congo red (CR) dye is a benzidine-based diazo anionic dye that is used extensively in the silk, wool, and textile as well as in food and pharmaceutical industries, and acidic conditions as an indicator.[12,13] CR is an organic pollutant with high toxicity and hard degradation due to its complicated aromatic construction. It is difficult to remove from water because it is very soluble in it. It possesses cancer-causing qualities and harms the skin, eyes, reproductive organs, and respiratory systems.[12,13] Dyes such as CR are structurally resistant to oxidation and subsequent biodegradation, thus they can remain in the environment for a long time. Therefore, it is very important to plan the color discharge in industrial wastewater.[14]

So far, several methods have been proposed for the decolorization of organic dye-contaminated water, such as surface adsorption, membrane filtration, electrochemical oxidation, biological purification, sono-catalysis, catalytic reduction, photo-Fenton process, degradation caused by

radiation, biological degradation and photocatalytic decomposition.[13,15] Conventional wastewater treatment methods are associated with some drawbacks. As for some of these methods like flocculation, coagulation, advanced oxidation, absorption, and precipitation, in addition to requiring long operation times, produce secondary slush that is costly to dispose of.[3]

Among the mentioned methods, the photocatalysis method is an environmentally friendly, low-cost, and sustainable process and it works by undergoing advanced oxidation processes.[6,12] Photocatalysis follows natural photosynthesis, which converts color molecules into harmless products such as CO_2 and H_2O by using light-absorbing substances.[6,16-19] Photocatalyst performance usually depends on electron-hole recombination rate, specific surface area, crystallite/grain size, defect sites, crystal structure, etc.[14] Metal oxides have significant stability and high photocatalytic activity.[20] Numerous researchers have created different kinds of photocatalysts over the last ten years including TiO_2,[21-23] CdS,[24] CeO_2,[25] ZnS[26], Fe_2O_3[27], MOFs[28,29], carbon quantum dots[30] and ZnO[31,32] which, because of their broad bandgap, primarily observe ultraviolet light-based photo absorption.[16] Ternary oxides with the chemical formula $A_xB_yO_z$ are compounds that have low band gap energy (where x, y, and z are various ratios of A, B, and O ions, respectively). In ternary metal oxides, more diverse types of metal can be selected than binary ones, and as a result, more effective photocatalysts can be synthesized, which can be modified by doping some metals to further control the band gap energy. One of these ternary oxide compounds is the cubic crystal structure of perovskite.[33-35] Perovskites have some advantages, such as good conductivity, crystal structures, simple oxygen and electron transformation, and photo-stability.[36,37] In particular, Sr_2TiO_4 as a Ruddlesden Popper-based layered perovskite, with a general formula of $AO–(ABO_3)_n$,[38] due to its exceptional thermal and chemical stability and superb optical characteristics, has proven a great perovskite-based photocatalyst.[36] Sr_2TiO_4 has a unique layered structure in which SrO layers alternate with TiO_2 layers. Its structure is stabilized by this configuration, which also affects its electrical and optical characteristics, making it a viable option for several uses.[39] The correlation between Sr_2TiO_4's optical and structural characteristics is incredibly complex and intriguing. The optical characteristics of Sr_2TiO_4 are largely determined by its layered structure, in which TiO^{-2} layers alternate with SrO layers. This particular configuration affects the electronic band structure and produces a broad bandgap of about 3.2 eV.[40,41] The material's capacity to absorb ultraviolet light, which qualifies it for photocatalytic applications, is due to its broad bandgap. The electronic transitions under light irradiation are directly influenced by structural characteristics, including bond lengths within the lattice and the coordination of Sr^{2+} ions.[42] For example, localized states within the bandgap can be caused by the existence of oxygen vacancies and the particular arrangement of TiO^{-6} octahedra, altering the absorption and emission properties.[43]

To improve Sr_2TiO_4's photocatalytic performance, research into doping techniques and composite production is necessary because of the material's low efficiency under visible light.[39] One effective way to increase Sr_2TiO_4's photocatalytic effectiveness is through nanostructuring. Because nanostructures have a higher surface area to volume ratio than other materials, they can improve light absorption and provide more photocatalytic reaction sites.[44]

From another point of view, one key tactic for managing the size, shape, and functional characteristics of nanostructures is the utilization of templates during their synthesis. Hard templates (anodic aluminum oxide, for example) or soft templates (surfactants, for example) operate as a scaffold to guide the formation of nanomaterials, producing highly ordered and consistent structures.[45] The form and surface properties of the resultant nanostructures are strongly influenced by the template selection. Hard templates, for example, provide exact control over size and structural stiffness, but soft templates permit a greater range of morphologies and flexibility.[46] This templating effect plays a key role in modifying the chemical and physical characteristics of nanostructures, improving their performance in a range of applications including energy storage, environmental remediation, and catalysis.[47] Other advantages of this heterogeneous catalyst, are easy catalyst separation, catalyst reusability, and no toxicity.[48]

To that end, in this study, the photocatalytic capacity of nanoscale Sr_2TiO_4 prepared by a sol-gel synthesis with some templates as a heterogeneous photocatalyst is investigated for the degradation of MT and CR dyes in aqueous solutions.

2. EXPERIMENTAL

Materials

Strontium(II) nitrate was bought from Aldrich. Titanium tetraisopropoxide, isopropanol, CR, acetylacetone, MB, polyethylene glycol, urea, starch, chitosan, ammonium carbonate and polyethylene glycol 20000 (PEG) were bought from Merck Chemical Company (Darmstadt, Germany) and without additional purification used.

Physical measurements

On a Philips PW1800 diffractometer samples' X-ray diffraction (XRD) patterns were captured using monochromatic Cu Kα radiation that had been nickel-filtered (λ = 0.15405 nm). The diffractograms were recorded in the 2Θ range of 4°-90° while the X-ray generator was operating at 40 kV and 30 mA. The powder diffraction file (PDF) database (JCPDS, International Centre for Diffraction Data) was used to determine the phases.

Fourier Transform Infrared Spectroscopy (FT-IR) spectra of the samples were obtained using a Bruker (Tensor 27) instrument using a KBr pellet in the region of 4000-400 cm^{-1} (10 mg sample and 200 mg powdered potassium bromide) under ambient conditions. A LEO 1455VP was utilized for scanning electron microscope (SEM) at an accelerated voltage of 10 kV. By measuring the intensity of dye absorption at the wavelength of maximum absorption using UV/Vis (Perkin Elmer, Lambda 35), dye concentration was calculated.

Catalyst synthesis method

In this study, the sol-gel method was employed to synthesize the Sr_2TiO_4 nano-photocatalyst using the modified previous method.[49] In a 100 mL reaction vessel, 20 mL of isopropanol was added first, followed by 0.01 mol of acetylacetone, 0.01 mol of titanium tetraisopropoxide, and a template. The used templates in different samples were 4.00 g of PEG, 4.00 g of ethylene glycol, 0.16 g of starch, 0.96 g of ammonium carbonate, 0.14 g of chitosan and 0.10 g of urea. Strontium(II) nitrate (0.01 mol) was then mixed with the resultant mixture and refluxed for 2 h. The combination that resulted was then heated to cause a gel to develop. The resulting gel was dried at 80 °C for 24 h, then calcined in air for 6 h at 900 °C.

Photocatalytic activity determination

In this study, the dye pollutant samples were CR and MB. 100 mL of dye (50 ppm) received 0.05 g of Sr_2TiO_4 nano-photocatalyst while being stirred. The pH of the MB solution was raised to 9 by adding NaOH (0.4 N). The light source was a UV lamp with a 55 W output. The Pyrex container holding the catalyst and dye had an 8 cm gap between it and the UV lamp. Throughout the experiment, air was bubbled into the solution to provide a steady source of dissolved oxygen. The setup was left in the dark for about 20 min before the radiation treatment to achieve an adsorption/desorption equilibrium. At regular intervals throughout the irradiation process, samples of the destroyed dye were taken and centrifuged. Next, the obvious solutions with a UV spectrophotometer were examined.

3. RESULTS AND DISCUSSION

Catalyst characterization

In this work, Sr_2TiO_4 nano-photocatalyst was synthesized by titanium tetraisopropoxide and template in the solution of acetylacetone and isopropanol followed by the addition of strontium(II) nitrate during reflux then was calcinated at 900 °C. The selected templates had previously shown positive results in nanoparticle synthesis, particularly as templates for the production of earth-alkaline nano oxides. The used templates are polyethylene glycol,[50] ethylene glycol,[51] starch,[52] ammonium carbonate,[53] chitosan[54] and urea.[55] The SEM of these photocatalysts were shown in Figure 1a-f and reveal the uniform morphology of spherical shapes with 90-100 nm particle size for PEG, 60 nm for ethylene glycol, 90 nm for starch and 100 nm for urea and 1 µm for ammonium carbonate and about 135 nm for chitosan templates.

For comparison of the effect of the template on the photocatalyst performance, degradation of CR after 40 min of illumination by all templated photocatalysts was investigated. According to Figure 2, the catalysis of Sr_2TiO_4 nanoparticles can degrade 75.0, 71.0, 62.0, 60.0, 53.0 and 51.0% of the CR by PEG, ethylene glycol, ammonium carbonate, starch, chitosan and urea as templates, respectively.

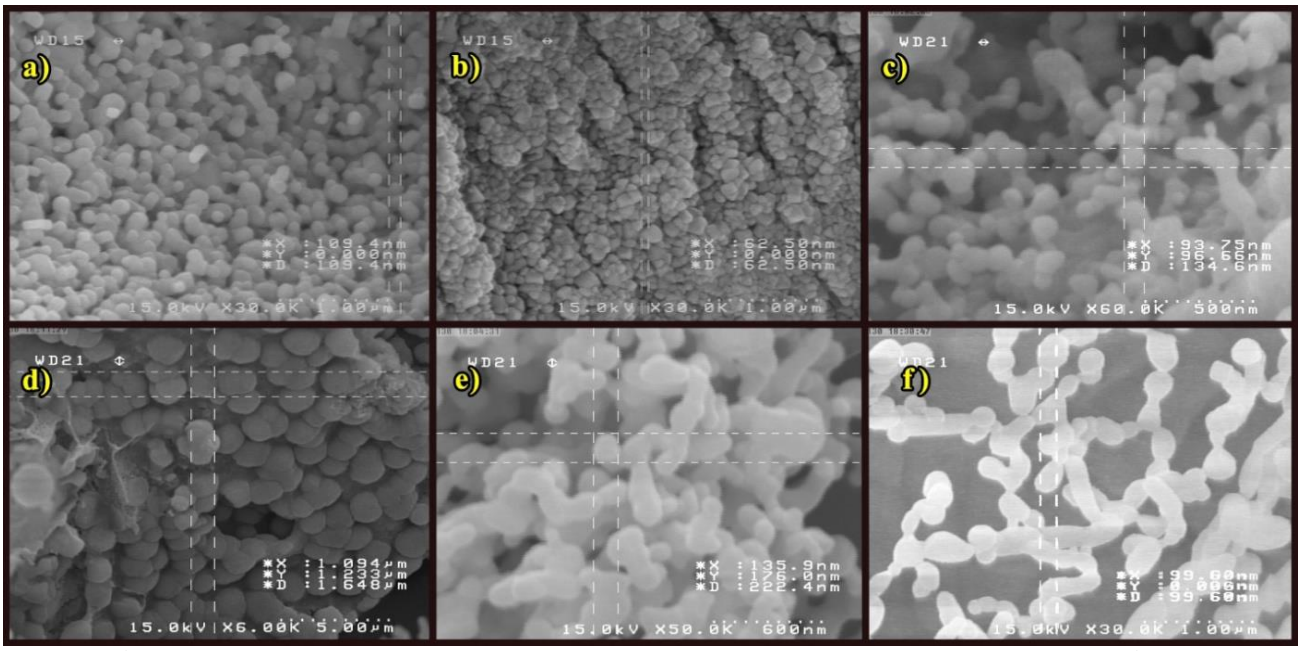

Figure 1. SEM of the photocatalyst synthesized by (a) PEG, (b) ethylene glycol, (c) starch, (d) ammonium carbonate, (e) chitosan and (f) urea as templates.

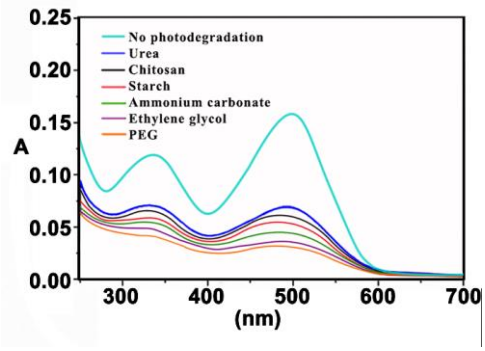

Figure 2. UV-vis spectra of 5 ppm of CR in aqueous Sr_2TiO_4 nano-photocatalyst dispersion which was synthesized by different templates at 40 min under UV irradiation.

The specific surface area was measured using the BET method and the pore size distribution was calculated using the classical Barrett-Joyner Halenda model.[56] As shown in Figure 3, the adsorption-desorption curves for the composite displayed type IV adsorption-desorption isotherms, which is a typical characteristic of mesoporous materials. The BET surface area of the PEG, ethylene glycol and urea were 112.1, 96.6 and 60.5 cm^3/g, respectively, which could be related to their average particle size. These results shows that there is a direct correlation between particle size and photocatalytic activity. Because the performance of these catalysts is close to each other, just PEG as the template for photocatalyst synthesis was chosen because of its high performance in the CR degradation process and its uniform nanostructure. That's why in the continuation of the work, the characterization of this photocatalyst has been investigated.

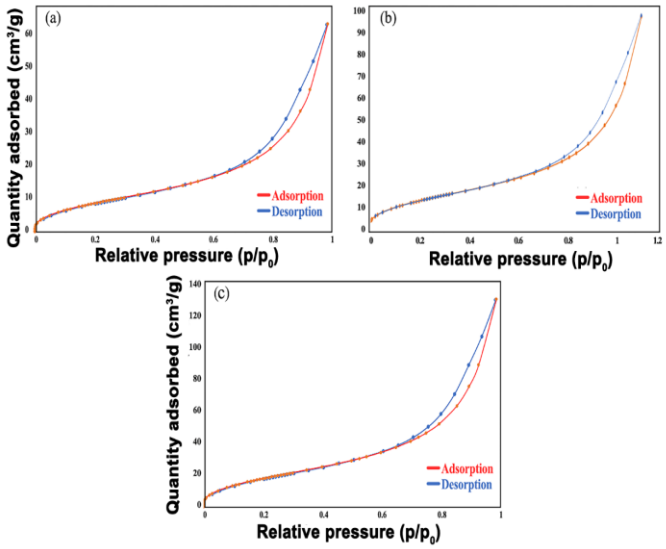

Figure 3. BET adsorption and desorption isotherm curve of catalyst templated by (a) PEG, (b) ethylene glycol and (c) urea.

The synthesized sample's XRD pattern (JCPDS PDF No. 39-1471) is depicted in Figure 4a and features the distinctive peaks of the Sr_2TiO_4 phase as the main product. As can be seen, the TiO_2 minor phase (Brookite, JCPDS PDF No. 29-1360) appears to be inconsequential in this pattern, with the Sr_2TiO_4 phase showing at d values of 2.850, 2.743, 2.101, 2.070, 1.941, and 1.606, respectively, corresponding to 103, 110, 006, 114, 200, and 213 reflections. The FT-IR spectrum of the nano-photocatalyst can be seen in Figure 4c. Appeared broad and strong peak appeared at 588 cm^{-1} refers to the stretching vibration of M-O and a peak at 471 cm^{-1}, which M-O bending normal Sr_2TiO_4 is responsible for being weaker but sharper. Absorption peaks at 858 and 1461 cm^{-1} appear, indicating carbonate formation because of CO_2 adsorption.[49] In Figure 4d, the TGA and DTA curves are displayed. TGA results show that constant mass is reached at temperatures over 590°C after 73.7% of the initial mass has been lost. The DTA curve consists of two main phases. The first step from 250 to 350°C with a weight loss of 51.3% is an exothermic peak due to the degradation of the PEG matrix releasing CO_2 gas.[57,58] The second weight loss is an endothermic peak around 540-600 °C encompassing a weight loss of 9.9% which is related to the initial melting of strontium(II) nitrate followed by its breakdown into nitrogen oxides and the creation of perovskite.[49,59]

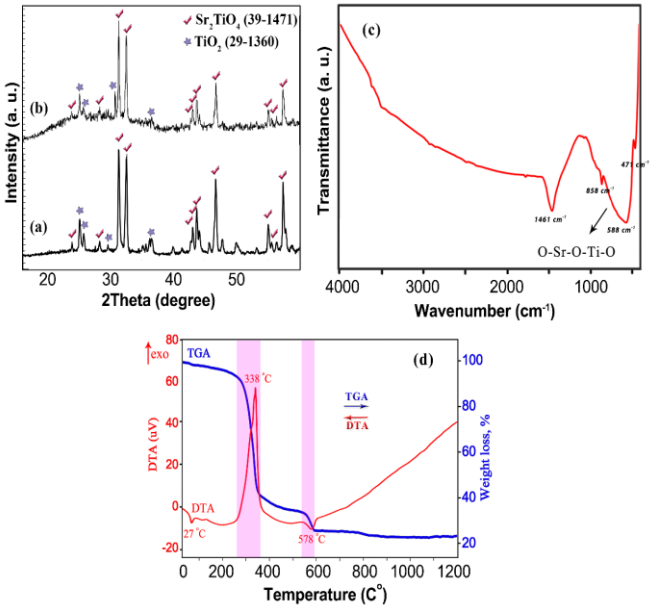

Figure 4. XRD pattern of Sr_2TiO_4 nano-photocatalyst (a) before and (b) after the degradation process, (c) FT-IR spectra of the Sr_2TiO_4 nano-photocatalyst (d) TGA and DTA curves of the Sr_2TiO_4 nano-photocatalyst.

Photo-catalytic evaluations

CR and MB are anionic and cationic dyes, respectively. The adsorption of the dye on the catalyst's surface aids in photodegradation and the electric charge properties of the catalyst and substrate are found to be crucial in the adsorption process. Nano TiO_2 exhibits amphoteric behavior in aqueous media. TiO_2's point of zero charge (pzc) occurs between pH 5.6 and 6.4.[60]

TiO_2 has a negatively charged surface at pH values higher than pH_{pzc}. The positively charged TiO_2 surface may efficiently adsorb the negatively charged dye anion and vice versa at lower pH values because the nano TiO_2 surface is in the protonated state. Because of this, in Layered perovskite Sr_2TiO_4 which there is TiO_2 in its skeleton, the photodegradation procedure was carried out at alkaline conditions, with pH = 9 for MB and pH = 5 for CR, in order to prevent dye adsorption on the perovskite surface. Maximum UV-vis absorptions at 497 nm for CR and 664 nm for MB were used to study photodegradation reactions.

After adding Sr_2TiO_4 nano-photocatalyst to the solution and before exposing it to UV light, it was kept in the dark for 20 min to reach equilibrium. The decrease in absorption in this step indicates the amount of dye adsorption on the surface of Sr_2TiO_4 nano-photocatalyst, which was estimated to be about 15.0% and 10.0% for CR and MB, respectively, under the conditions used.

The degree of dye decolorization can be determined using the formula C (%) = $(A_0 - A)/A_0 \times 100$, where C is the decolorization degree, and A_0 and A are the absorptances of dye solution before and after photo-catalysis, respectively. The plots of the degradation versus time are displayed in Figure 5a-b.

According to Figure 5a-b, the catalysis of Sr_2TiO_4 nano-photocatalyst can successfully degrade 94.0% of the CR and about 97.0% of the MB after 60 min of illumination.

Numerous researchers have verified that the Langmuir-Hinshelwood kinetic expression serves as the kinetic model for heterogeneous photocatalysis.[61,62]

$$r = dC/dt = kKC/1 + KC \qquad (1)$$

Where k is the reaction rate constant (mg L^{-1} min^{-1}), r is the reactant's oxidation rate (mg L^{-1} min^{-1}), C is its concentration (mg L^{-1}), t is the illumination time, and K is its adsorption coefficient (L mg^{-1}). The aforementioned equation can be condensed to an apparent first-order equation when the chemical concentration C_0 is small:

$$Ln(C_0/C) = kt \qquad (2)$$

Where C_0 and C, respectively, are the dye concentrations at zero time and time t. The slope of the straight line that results from linear regression and the plot of LnC_0/C against time matches the apparent first-order rate constant k.

Figure 5c-d display the graphs of $Ln(C_0/C)$ vs. irradiation time for CR and MB. The regression coefficient R was 0.99424 for CR and 0.98054 for MB, which suggested the photodegradation by Sr_2TiO_4 nano-photocatalyst fit the Langmuir–Hinshelwood kinetic expression well.

Based on the slope of the $Ln(C_0/C)$ against time plots under optimal conditions, rate constants for CR and MB were calculated to be 0.046 min^{-1} and 0.023 min^{-1}, respectively.

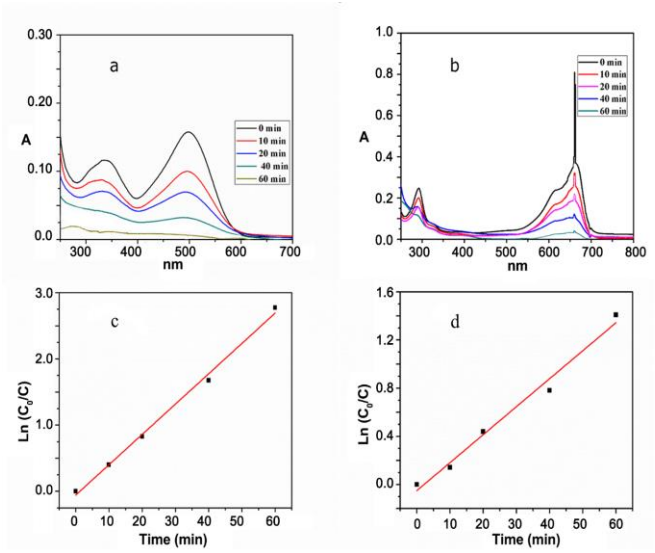

Figure 5. UV-vis spectra of 5 ppm of (a) CR and (b) MB in aqueous Sr_2TiO_4 nano-photocatalyst dispersion at various times under UV irradiation, (c) Plot of $Ln(C_0/C)$ versus T for CR and (d) for MB.

Under UV light irradiation, the primary control experiment was performed without Sr_2TiO_4 nano-photocatalyst powder. Figure 6 shows the plots of percent degradation (x) vs. irradiation time (min) at 497 nm for the aqueous suspension of CR and 664 nm for MB with and without synthesized Sr_2TiO_4 nano-photocatalyst under UV light.

It demonstrates that the synthesized Sr_2TiO_4 nano-photocatalyst has a high efficiency of 94% in CR decolorization and 97% in MB decolorization after 60 min but without Sr_2TiO_4 nano-photocatalyst, only a slow decrease in the concentration of CR and MB was detected under UV irradiation revealing that photolysis can be neglected compared with the photocatalyst.

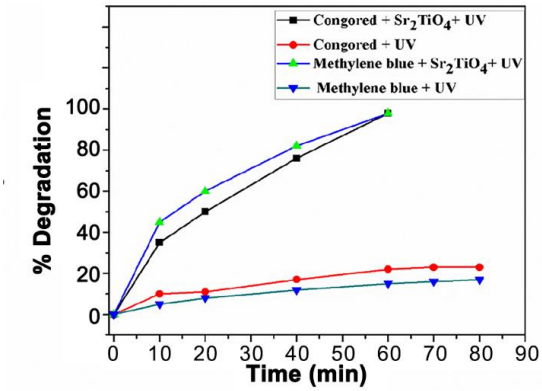

Figure 6. Efficiency of photodegradation (%) as a function of time CR and MB at 497 nm and 664 nm respectively.

Mechanism of photocatalytic degradation of dyes

Figure 7 shows a possible mechanism of the dye degradation reaction of semiconductor photocatalysts. The estimated value of band gap energy for similar Sr_2TiO_4 nano-photocatalyst is about 4 eV.[63] When the energy of the incoming photon surpasses the photocatalyst's bandgap, electrons (e^-) move from the valence band to the conduction band, leaving positively charged holes (h^+) behind in the valence band. As a result, an electron-hole pair is created.[64] The superoxide radical anions ($O_2^{\cdot-}$) are produced when the photoexcited electrons of the conduction band undergo reduction interaction with electron acceptors such as O_2 dissolved in water or with the oxygen from the Sr_2TiO_4 nano-photocatalyst surface. The photogenerated holes oxidize OH^- or H_2O adsorbed on the catalyst surface into $OH\cdot$ radicals when they interact with them. These redox-active species, which include superoxide radical anions ($O_2^{\cdot-}$), hydroxyl radicals ($OH^{\cdot}$), and holes (h^+), may break down the organic molecules into innocuous compounds, such as CO_2 and H_2O.[65,66]

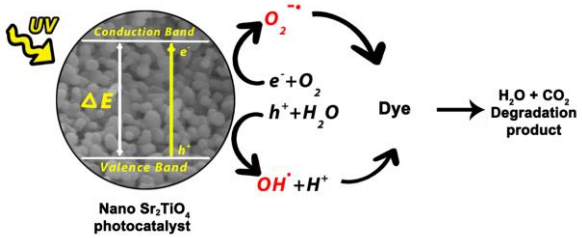

Figure 7. Mechanism of the dye degradation reaction of semiconductor photocatalysts.

Stability of catalyst

Five consecutive cycles of CR and MB degradation under UV light were used to verify the catalyst's stability. The results are given in Figure 8a and b. In five cycles, the degradation efficiencies have not shown a noticeable decrease. This demonstrated the remarkable reusability of Sr_2TiO_4 nano-photocatalyst. Also, as seen in Figure 4b, the XRD pattern of Sr_2TiO_4 nano-photocatalyst before and after the reaction not much has changed during the irradiation and degradation process.

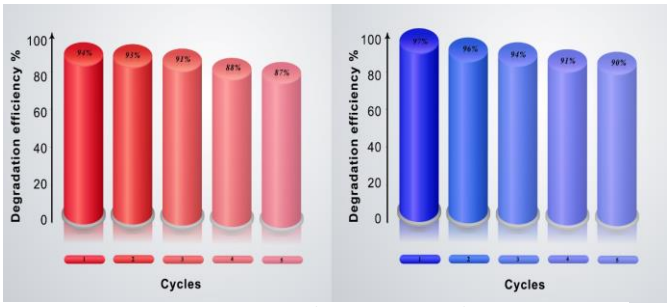

Figure 8. The reusability charts of photocatalysts for (a) CR and (b) MB.

Comparison of Nano Sr_2TiO_4 catalytic activity with those reported previously

Tables 1 and 2 provide details on the comparative study of several previously reported nano-photocatalysts with this work. Most selective catalysts are ternary metal oxides. The degraded dye in Table 1 is CR and in Table 2 is MB. Compared to other works, if all effective factors are considered, it is clear that the present catalyst has shown higher potential and excellent activity for photodegradation than other catalysts. The amount of catalyst used and the irradiation time are less than in other works, and on the other hand, the used dye concentration is higher.

Table 1. Comparison of nano Sr_2TiO_4 nano-photocatalyst activity and previously reported literature for degradation of CR

Catalyst	Catalyst amount (g L^{-1})	Time (min)	CR (mg L^{-1})	Degradation (%)	k (min^{-1})	Light	References
Nano Sr_2TiO_4	0.005	60	50.0	94.0	0.046	UV	present work
$NiMn_2O_4$	0.005	120	5.0	62.0	0.023	Visible light	67
ZnO/Ag–Ag_2O	0.8	80	40.0	96.3	0.041	UV	12
WO_3–TiO_2/AC	10.0	120	40.0	95.2	0.026	UV	68
Ce-doped $BaTiO_3$	0.3	120	5.0	78.5	0.0117	UV	69
ZnS–Co^{2+}	0.8	120	10.0	94.0	0.022	UV	70
$SrFe_{12}O_{19}$	0.5	180	13.9	90	-	Visible light	71

Table 2. Comparison of nano Sr_2TiO_4 photo-catalytic activity and previously reported literature for degradation of MB

Catalyst	Catalyst amount (g L^{-1})	Time (min)	MB (mg L^{-1})	Degradation (%)	k (min^{-1})	Light	References
Nano Sr_2TiO_4	0.005	60	50.0	97.0	0.023	UV	Present work
ZnO/Ag–Ag_2O	0.8	80	10.0	97.5	0.076	UV	[12]
$NiMn_2O_4$	0.005	120	5.0	92.0	0.154	Visible light	[67]
CeO_2/GO/PAM	0.25	90	5.0	90.0	0.025	UV	[9]
Pt/WO_3–GO	0.5	70	3.20	94.0	-	Visible light	[72]

4. CONCLUSION

This work studied photocatalytic degradation of CR and MB by perovskite Sr_2TiO_4 nano-photocatalyst as photocatalyst. The catalyst was made using the sol-gel method, polyethylene glycol 20000 was used as a template and it was then calcined at 900 °C. The particle size of uniform spherical catalyst was 90-100 nm. The degradation efficiency of 94.0% for CR and 97.0% for MB was achieved at room temperature, 5 ppm of Sr_2TiO_4 nano-photocatalyst dosage, 50 mg L^{-1} initial dye concentration, and 60 min irradiation time. This photocatalyzed reaction exhibits a first-order behavior. The degradation rate constants are 0.023 min^{-1} and 0.046 min^{-1} for MB and CR, respectively. Since the photocatalyst was reused at least five times without any additional treatment, it demonstrated remarkable stability and reusability. In conclusion, we have developed a photocatalyst that offers a high potential for MB and CR photocatalytic degradation.

CONFLICTS OF INTEREST

The authors declare that there are no conflicts of interest.

ACKNOWLEDGMENTS

The Universities of Farhangian and Alzahra's assistance is sincerely thanked.

AUTHOR INFORMATION

Corresponding Author

Elnaz Rashtizadeh: Email: e.rashtizadeh@cfu.ac.ir. *ORCID*: 0009-0008-8572-4978

Author

Zeinab Asgharpour

REFERENCES

1. S. Mishra, N. Chakinala, A. G. Chakinala, P. K. Surolia, *Catal. Commun.* **2022**, *171*, 106518.
2. M. Kumar, R. Vaish, Z. M. Elqahtani, I. Kebaili, M. S. Al-Buriahi, T. H. Sung, W. Hwang, A. Kumar, *J. Mater. Res. Technol.* **2022**, *21*, 1998-2012.
3. S. A. Kumar, M. Jarvin, S. S. R. Inbanathan, A. Umar, N. P. Lalla, N. Y. Dzade, H. Algadi, Q. I. Rahman, S. Baskoutas, *Environ. Technol. Innov.* **2022**, *28*, 102746.
4. H. Bayahia, *J. Saudi Chem. Soc.* **2022**, *26*, 101432.
5. S. Thulasi Karunakaran, R. Pavithran, M. Sajeev, S. Mohan Mohan Rema, *Results Chem.* **2022**, *4*, 100504.
6. C. Mun, M. Mansoob, M. Yusuf, A. Khan, *Chem. Phys. Impact* **2022**, *4*, 100082.
7. M. Berradi, R. Hsissou, M. Khudhair, M. Assouag, O. Cherkaoui, A. El, A. El, **2019**, *5*, 1-11.
8. U. Shanker, *Environ. Chem. Lett.* **2017**, *15*, 623-642.
9. O. Polyacrylamide, Z. Kalayc, O. Bengu, O. Pekcan, F. B. Erim, **2023**, *8*, 13004-13015.
10. E. A. Abdelrahman, R. M. Hegazey, S. H. Ismail, H. H. El-feky, A. M. Khedr, M. Khairy, A. M. Ammar, *Arab. J. Chem.* **2022**, *15*, 104372.
11. A. Subaihi, A. M. Naglah, *Arab. J. Chem.* **2022**, *15*, 103613.
12. Y. Su, X. Zhao, Y. Bi, X. Han, *Clean Technol. Environ. Policy* **2019**, *21*, 367-378.
13. N. Hokonya, C. Mahamadi, N. Mukaratirwa-Muchanyereyi, T. Gutu, C. Zvinowanda, *Heliyon* **2022**, *8*, e10277.
14. G. V. Geetha, R. Sivakumar, C. Sanjeeviraja, V. Ganesh, *J. Sol-Gel Sci. Technol.* **2021**, *97*, 572-580.
15. E. Shi, X. Wang, M. Zhang, X. Wang, J. Gao, Y. Zheng, X. Zhu, *Int. J. Electrochem. Sci.* **2022**, *17*, 221242.
16. C. Kumari, P. Sharma, S. C. Katyal, M. Tanwar, P. Bamola, H. Sharma, R. Kumar, S. Chhoker, *Results in Surfaces and Interfaces* **2022**, *9*, 100088.
17. R. Nejat, M. Halimi Khalil Abad, Z. Gholizadeh, *Inorg. Chem. Res.* **2024**, *8*, 52-58.
18. S. Saeednia, P. Iranmanesh, T. Shabani, *Inorg. Chem. Res.* **2024**, *8*, 1-7.
19. F. Kazemi, H. A. Zamani, M. R. Abedi, M. Ebrahimi, *Inorg. Chem. Res.* **2022**, *6*, 31-38.
20. P. B. Sreelekshmi, R. R. Pillai, S. Unnimaya, A. L. Anju, A. P. Meera, *Clean Technol. Environ. Policy* **2023**, *26*, 3805-3818.
21. A. S. M. Nur, M. Sultana, A. Mondal, S. Islam, F. N. Robel, A. Islam, M. S. A. Sumi, *J. Water Process Eng.* **2022**, *47*, 102728.
22. S. Mottola, A. Mancuso, O. Sacco, I. De Marco, V. Vaiano, *J. Supercrit. Fluids* **2022**, *188*, 105695.
23. E. Gholamrezapor, A. Eslami, *Inorg. Chem. Res.* **2021**, *5*, 19-36.
24. A. Singh, D. Singh, B. Ahmed, A. K. Ojha, *Mater. Chem. Phys.* **2022**, *277*, 125531.
25. K. B. Kusuma, M. Manju, C. R. Ravikumar, N. Raghavendra, M. A. S. Amulya, H. P. Nagaswarupa,

H. C. A. Murthy, M. R. A. Kumar, T. R. Shashi Shekhar, *Appl. Surf. Sci. Adv.* **2022**, *11*, 100304.
26. S. Ahluwalia, N. T. Prakash, R. Prakash, B. Pal, *Chem. Eng. J.* **2016**, *306*, 1041-1048.
27. L. Huang-Mu, S. Devanesan, K. Farhat, W. Kim, G. Sivarasan, *Chemosphere* **2023**, *337*, 139229.
28. S. Ghanei-Zare, M. Moghadasi, R. Khajavian, N. Akbarzadeh-T, M. Mirzaei, *J. Mol. Struct.* **2023**, *1286*, 135563.
29. A. Haziq, A. Gholipour, S. Farhadi, *Inorg. Chem. Res.* **2024**, *8*, 32-45.
30. M. Rezaeia, A. Hekmat, J. Chamani, K. Sadri, M. Darroudi, *Inorg. Chem. Res.* **2022**, *6*, 107-113.
31. A. Haziq, A. Gholipour, S. Farhadi, *Inorg. Chem. Res.* **2024**, *8*, 32-45.
32. S. Ghanei-Zare, M. Moghadasi, R. Khajavian, N. Akbarzadeh-T, M. Mirzaei, *J. Mol. Struct.* **2023**, *1286*, 135563.
33. M. Rezaeia, A. Hekmat, J. Chamani, K. Sadri, M. Darroudi, *Inorg. Chem. Res.* **2022**, *6*, 107-113.
34. M. Rashid Al-Mamun, M. Shofikul Islam, M. Rasel Hossain, S. Kader, M. Shahinoor Islam, M. Zaved Hossain Khan, *Environ. Nanotechnology, Monit. Manag.* **2021**, *16*, 100495.
35. L. Kaliraj, J. C. Ahn, E. J. Rupa, S. Abid, J. Lu, D. C. Yang, *J. Photochem. Photobiol. B Biol.* **2019**, *199*, 111588.
36. C. M. Khor, M. M. Khan, M. Y. Khan, A. Khan, M. H. Harunsani, *J. Saudi Chem. Soc.* **2022**, *26*, 101534.
37. K. V Ivanov, A. V Plotvina, A. V Agafonov, *Russ. J. Inorg. Chem.* **2023**, *68*, 104-114.
38. S. A. Kurnosenko, O. I. Silyukov, I. A. Rodionov, Y. P. Biryukov, A. A. Burov, I. A. Zvereva, *Russ. J. Inorg. Chem.* **2023**, *68*, 1903-1912.
39. J. Wang, N. Li, Y. Tang, Y. He, K. Shan, *Int. J. Electrochem. Sci.* **2022**, *17*, 22081.
40. M. Zhou, J. Chen, Y. Zhang, M. Jiang, S. Xu, Q. Liang, Z. Li, *J. Alloys Compd.* **2020**, *817*, 152796.
41. A. Vijay, K. Bairagi, S. Vaidya, *Mater. Adv.* **2022**, *3*, 5055-5063.
42. J. Yang, J. Pang, X. Luo, L. Ao, Q. Xie, X. Wang, H. Yang, X. Tang, *Materials (Basel).* **2023**, *16*, 5195, 1-12.
43. A. Mittal, R. Baranwal, P. Kumar, S. Upadhyay, *Emergent Mater.* **2024**, *7*, 1763-1777.
44. Y. Wang, Y. Tan, H. Wang, Y. Cen, J. Ma, Q. Ruan, L. Wang, J. Cai, *J. Mater. Sci. Mater. Electron.* **2024**, *35*, 1058.
45. H. A. Gatea, S. J. Shoja, H. J. Albazoni, *JOM* **2023**, *75*, 4470-4478.
46. J. Hu, Z. Ma, R. Sa, Y. Zhang, K. Wu, *Phys. Chem. Chem. Phys.* **2017**, *19*, 15120-15128.
47. P. Villars, K. Cenzual, Eds. , **n.d.**
48. X. Ye, Y. Jiang, X. Chen, B. Guo, S. Mao, Y. Guo, C. Zhao, *Front. Energy Res.* **2022**, *10*, 964011.
49. J. Xu, X. Zhu, L. Xu, C. Kan, D. Shi, *Nanoscale* **2023**, *15*, 1687-1694.
50. M. Pasquali, J. Liang, S. Shivkumar, *Nanotechnology* **2011**, *22*, 375605.
51. F. Farzaneh, B. Dashtipour, E. Rashtizadeh, *J. Sol-Gel Sci. Technol.* **2017**, *81*, 859-866.
52. E. Rashtizadeh, F. Farzaneh, *J. Taiwan Inst. Chem. Eng.* **2013**, *44*, 917-923.
53. E. Rashtizadeh, F. Farzaneh, Z. Talebpour, *Bioresour. Technol.* **2014**, *154*, 32-37.
54. M. Inada, N. Enomoto, K. Hayashi, J. Hojo, S. Komarneni, *Ceram. Int.* **2015**, *41*, 5581-5587.
55. H. Chen, X. Mu, Y. Jiang, Z. He, *J. Phys. Conf. Ser.* **2024**, *2713*, 12038.
56. N. Sutradhar, A. Sinhamahapatra, S. Pahari, M. Jayachandran, B. Subramanian, H. C. Bajaj, A. B. Panda, *J. Phys. Chem. C* **2011**, *115*, 7628-7637.
57. T. Linda, S. Muthupoongodi, X. S. Shajan, S. Balakumar, *Optik (Stuttg).* **2016**, *127*, 8287-8293.
58. I. Ercan, O. Kaygili, T. Ates, B. Gunduz, N. Bulut, S. Koytepe, I. Ozcan, *Ceram. Int.* **2018**, *44*, 14523-14527.
59. M. Yang, Y. Wang, *Langmuir* **2024**, *40*, 20368-20378.
60. C. P. Dhanalakshmi, *Int. J. Phys. Sci.* **2012**, *7*, 2093-2101.
61. X. Qiao, M. Bai, K. Tao, X. Gong, R. Gu, H. Watanabe, K. Sun, J. Wu, X. Kang, *Nihon Reoroji Gakkaishi* **2010**, *38*, 23-30.
62. S. G. Hosseini, A. Eslami, *J. Therm. Anal. Calorim.* **2010**, *101*, 1111-1119.
63. R. Terzian, N. Serpone, *J. Photochem. Photobiol. A Chem.* **1995**, *89*, 163-175.
64. J. B. De Heredia, J. Torregrosa, J. R. Dominguez, J. A. Peres, *J. Hazard. Mater.* **2001**, *83*, 255-264.
65. C. -S. Chiou, J. -L. Shie, C. -Y. Chang, C. -C. Liu, C. -T. Chang, *J. Hazard. Mater.* **2006**, *137*, 1123-1129.
66. A. Sorkh-Kaman-Zadeh, A. Dashtbozorg, *J. Mol. Liq.* **2016**, *223*, 921-926.
67. C. Xu, G. P. Rangaiah, X. S. Zhao, *Ind. Eng. Chem. Res.* **2014**, *53*, 14641-14649.
68. M. G. Kim, J. E. Lee, K. S. Kim, J. M. Kang, J. H. Lee, K. H. Kim, M. Cho, S. G. Lee, *New J. Chem.* **2021**, *45*, 3485-3497.
69. K. Indira, S. Shanmugam, A. Hari, S. Vasantharaj, S. Sathiyavimal, K. Brindhadevi, A. El Askary, A. Elfasakhany, A. Pugazhendhi, *Environ. Res.* **2021**, *202*, 111647.
70. M. John Abel, A. Pramothkumar, V. Archana, N. Senthilkumar, K. Jothivenkatachalam, J. Joseph Prince, *Res. Chem. Intermed.* **2020**, *46*, 3509-3525.
71. J. Sun, Y. Wang, R. Sun, S. Dong, *Mater. Chem. Phys.* **2009**, *115*, 303-308.
72. P. Senthilkumar, D. A. Jency, T. Kavinkumar, D.

Dhayanithi, S. Dhanuskodi, M. Umadevi, S. Manivannan, N. V. Giridharan, V. Thiagarajan, M. Sriramkumar, K. Jothivenkatachalam, *ACS Sustain. Chem. Eng.* **2019**, *7*, 12032-12043.
73. H. R. Pouretedal, H. Beigy, M. H. Keshavarz, *Environ. Technol.* **2010**, *31*, 1183-1190.
74. O. Mohanta, Y. N. Singhbabu, S. K. Giri, D. Dadhich, N. N. Das, R. K. Sahu, *J. Alloys Compd.* **2013**, *564*, 78-83.
75. A. A. Ismail, M. Faisal, A. Al-haddad, *J. Environ. Sci.* **2017**, *66*, 328-337.